



# Respiratory-gated PET imaging with reduced acquisition time for suspect malignancies: the first experience in application of total-body PET/CT

Guobing Liu<sup>1,2,3,4</sup> · Shuguang Chen<sup>1,2,3,4</sup> · Yan Hu<sup>1,2,3,4</sup> · Shuangliang Cao<sup>5</sup> · Xinlan Yang<sup>5</sup> · Yun Zhou<sup>5</sup> · Hongcheng Shi<sup>1,2,3,4</sup>

Received: 9 July 2022 / Revised: 8 September 2022 / Accepted: 8 December 2022 / Published online: 24 December 2022  
© The Author(s), under exclusive licence to European Society of Radiology 2022

## Abstract

**Objectives** This study aimed to investigate the performance of respiratory-gating imaging with reduced acquisition time using the total-body positron emission tomography/computed tomography (PET/CT) scanner.

**Methods** Imaging data of 71 patients with suspect malignancies who underwent total-body 2-[<sup>18</sup>F]-fluoro-2-deoxy-D-glucose PET/CT for 15 min with respiration recorded were analyzed. For each examination, four reconstructions were performed: Ungated-15, using all coincidences; Ungated-5, using data of the first 5 min; Gated-15 using all coincidences but with respiratory gating; and Gated-6 using data of the first 6 min with respiratory gating. Lesions were quantified and image quality was evaluated; both were compared between the four image sets.

**Results** A total of 390 lesions were found in the thorax and upper abdomen. Lesion detectability was significantly higher in gated-15 (97.2%) than in ungated-15 (93.6%,  $p = 0.001$ ) and ungated-5 (92.3%,  $p = 0.001$ ), but comparable to Gated-6 (95.9%,  $p = 0.993$ ). A total of 131 lesions were selected for quantitative analyses. Lesions in Gated-15 presented significantly larger standardized uptake values, tumor-to-liver ratio, and tumor-to-blood ratio, but smaller metabolic tumor volume, compared to those in Ungated-15 and Ungated-5 (all  $p < 0.001$ ). These differences were more obvious in small lesions and in lesions from sites other than mediastinum/retroperitoneum. However, these indices were not significantly different between Gated-15 and Gated-6. Higher, but acceptable, image noise was identified in gated images than in ungated images.

**Conclusions** Respiratory-gating imaging with reduced scanning time using the total-body PET/CT scanner is superior to ungated imaging and can be used in the clinic.

## Key Points

- In PET imaging, respiratory gating can improve lesion presentation and detectability but requires longer imaging time.
- This single-center study showed that the total-body PET scanner allows respiratory-gated imaging with reduced and clinically acceptable scanning time.

**Keywords** 2-[<sup>18</sup>F]-fluoro-2-deoxy-D-glucose · Positron emission tomography · Respiratory gating · Malignant tumor

---

Guobing Liu and Shuguang Chen contributed equally to this article.

✉ Hongcheng Shi  
shi.hongcheng@zs-hospital.sh.cn

<sup>1</sup> Department of Nuclear Medicine, Zhongshan Hospital, Fudan University, No. 180 in Fenglin Road, Shanghai 200032, China

<sup>2</sup> Institute of Nuclear Medicine, Fudan University, Shanghai 200032, China

<sup>3</sup> Shanghai Institute of Medical Imaging, Shanghai 200032, China

<sup>4</sup> Cancer Prevention and Treatment Center, Zhongshan Hospital, Fudan University, Shanghai 200032, China

<sup>5</sup> Central Research Institute, United Imaging Healthcare Group Co., Ltd., Shanghai 201807, China

## Abbreviations

AFOV	Axial field of view
MTV	Metabolic tumor volume
PET/CT	Positron emission tomography/computed tomography
SNR	Signal-to-noise ratio
SUV	Standardized uptake value
TBR	Tumor-to-blood ratio
TLR	Tumor-to-liver ratio
VOI	Volume of interest

## Introduction

Respiratory motion affects positron emission tomography/computed tomography (PET/CT) image quality, because the acquisition time of PET (2–3 min/bed position) is much longer than the respiratory cycle time (3–6 s) [1]. The common problems are reduced image resolution, underestimation of the standardized uptake value (SUV), overestimation of tumor volume, and deformation or inaccurate localization of lesions [2].

Although respiratory gating can increase lesion SUV [3], decrease metabolic tumor volume (MTV) [4], reduce image noise, and improve diagnostic performance [5], it is generally not used in the clinic, because of the long imaging time required to match the count and image quality to non-gated imaging [6, 7]. The extended acquisition time is poorly tolerated by patients, and the time taken for the transfer and reconstruction of large data reduces working efficiency.

The advent of PET scanners with a long axial field of view (AFOV) such as the uEXPLORER (AFOV: 194 cm; United Imaging Healthcare) [8] and the Quadra (AFOV: 106 cm, Siemens Healthineers) [8], has significantly improved detector sensitivity and PET image quality. These scanners have enabled PET imaging with reduced acquisition time [9, 10], low tracer activity [9, 11], and delayed imaging time [12]. We hypothesized that the improved efficiency in count detection and the long AFOV would improve efficiency in respiratory-gated imaging too. In this study, we aimed to investigate whether respiratory-gated total-body PET imaging using the uEXPLORER could minimize the effect of respiratory motion and reduce acquisition time. The hardware-based technique was used since it is still the standard method for respiratory gating.

## Materials and methods

This study was approved by the Institutional Review Board of Zhongshan Hospital, Fudan University (B2021-329). Written informed consent was obtained from all patients.

## Patients enrollment

From September to December 2021, a total of 145 patients underwent respiratory-gating total-body [ $^{18}\text{F}$ ]FDG PET/CT for suspected malignancies in the thorax and upper abdomen. After an initial review of PET/CT images, 49 patients were excluded (15 had no lesions identified, 22 had lesions with invisible [ $^{18}\text{F}$ ]FDG uptake compared to the surrounding background, 7 had tumors that were not in the thorax and upper abdomen). Another five patients were excluded because of failure in lesion segmentation on PET images, including lesions that were close to the myocardium ( $n = 1$ ) or the stomach ( $n = 1$ ) which had obvious physiological uptake of [ $^{18}\text{F}$ ]FDG, and lesions that were too close to the segment from each other ( $n = 3$ ). Then, the remaining 96 patients were followed up, of which 25 patients without a pathologically confirmed diagnosis were excluded (Fig. 1). Finally, a total of 71 patients with pathologically confirmed malignancies ( $n = 68$ ) and benign lesions ( $n = 3$ ) were included.

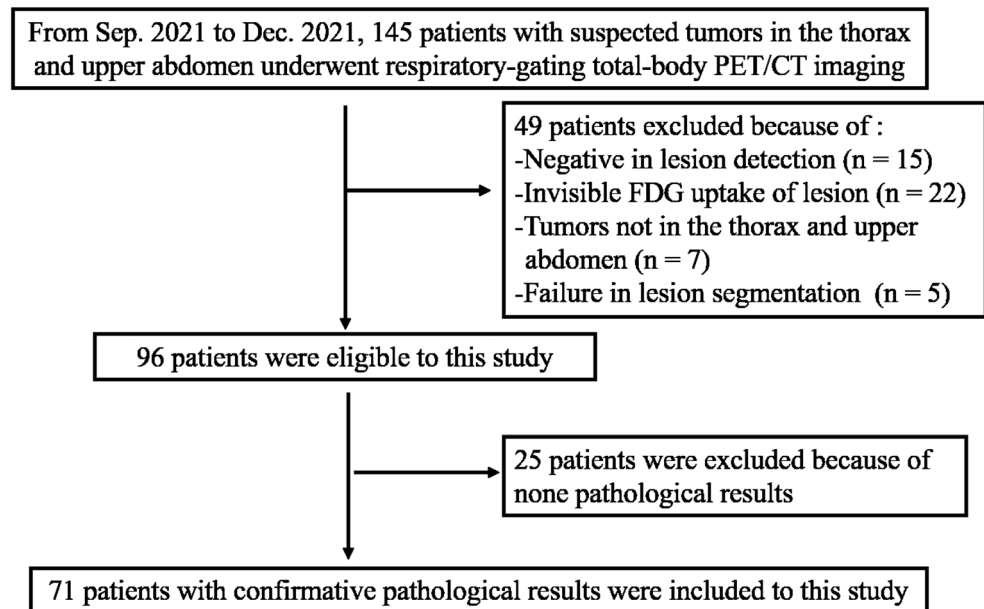
## Total-body PET/CT acquisition

Patients were fasted for at least 6 h before injection of  $^{18}\text{F}$ -FDG (4.4 MBq/kg). The mean glycemia of patients at the time of [ $^{18}\text{F}$ ]FDG injection was 6.1 (range: 3.9–10.7) mmol/L. Total-body PET/CT using the uEXPLORER scanner was performed after the patient had rested for about 60 min. The respiratory motion signal was recorded using a Vital Signal Monitor Gating belt (United Imaging Healthcare). Free-breathing CT acquisitions were performed using the following parameters: tube current, 140 mAs; tube voltage, 120 kV; collimation,  $64 \times 0.5$  mm; pitch, 1.0; and matrix,  $512 \times 512$ .

## Respiratory gating and PET image reconstruction

Each respiratory cycle was evenly divided into three bins with the second being taken to reconstruct respiratory-gated images, corresponding to the end-expiratory phase. In other words, approximately one-third of coincidences were extracted for a gated reconstruction. For comparison, four datasets of PET were reconstructed: gated and ungated reconstruction using the entire 15-min data (Gated-15 and Ungated-15), ungated reconstruction using the first 5 min (Ungated-5), and gated reconstruction using the first 6 min (Gated-6). Ungated-5 was reconstructed mainly for count-matched comparison with Gated-15. Gated-6 was reconstructed to investigate the performance of time-reduced respiratory-gated imaging, took into account an effective count equal to the standard protocol of 2 min/bed position recommended in the European guideline [13]. All PET image reconstructions were performed using the list-mode ordered-subsets expectation-maximization algorithm, incorporating time-of-flight and

**Fig. 1** Flowchart of patient enrollment



point-spread function with three iterations, 20 subsets, an image matrix of  $192 \times 192$ , and a slice thickness of 1.443 mm.

### Objective assessment of image quality and lesion demonstration

An objective assessment of image quality was performed by measuring the  $^{18}\text{F}$ FDG uptake in the background liver and the blood pool. Briefly, spherical volumes of interest (VOI) with diameters of 3 cm were placed in the middle area of the right lobe of the liver, and spherical VOIs as large as possible were drawn in the descending aorta without touching its wall. From each VOI, the maximum, mean, and standard deviation of standardized uptake value ( $\text{SUV}_{\text{max}}$ ,  $\text{SUV}_{\text{mean}}$ , and  $\text{SUV}_{\text{SD}}$ , respectively), corrected by the body weight, were estimated. The signal-to-noise ratio (SNR) of the liver and blood pool were calculated by dividing  $\text{SUV}_{\text{mean}}$  with  $\text{SUV}_{\text{SD}}$ . Identical VOIs were copied among the four image sets of each patient.

Lesions detectability was assessed by counting the number of lesions on the four image sets and comparing the number with the lesion count on chest high-resolution CT, enhanced abdominal CT, or MRI performed within 1 week before or after PET. For measuring the  $^{18}\text{F}$ FDG uptake in lesions, an adaptive threshold segmentation method was used to segment each lesion [14]. This segmentation method is a combination of the threshold algorithm and the region-growing algorithm, with the former finding an optimal threshold through iteration for lesion segmentation and the latter connecting the seed pixels and those pixels whose intensity values are greater than the optimal, to finally generate the lesion region [14, 15]. Making full use of the information from signal to background, this method showed better performance in lesion delineation

and is independent to image properties, scanner type, reconstruction, and imaging noise, compared to the commonly used relative or absolute fixed SUV threshold [14, 15]. MTV, peak SUV ( $\text{SUV}_{\text{peak}}$ ),  $\text{SUV}_{\text{max}}$ , and  $\text{SUV}_{\text{mean}}$  of the lesions were recorded.  $\text{SUV}_{90\%}$  was determined by averaging the SUV of voxels with  $\text{SUV} > 90\%$  of  $\text{SUV}_{\text{max}}$ . The tumor-to-liver ratio (TLR) and tumor-to-blood ratio (TBR) were calculated by dividing tumor  $\text{SUV}_{\text{max}}$  with  $\text{SUV}_{\text{mean}}$  of background liver and blood pool, respectively. All lesions were measured if there were fewer than then; otherwise, three lesions with the highest  $^{18}\text{F}$ FDG uptake were measured. Two operators (S.C. and G.L.) performed the quantitative measurements independently for testing inter-operator agreements, with one (S.C.) performing the measurements twice for testing intra-operator agreements.

### Subjective assessment of image quality

With the four data sets arranged side by side, two nuclear medicine physicians (Y.H. and G.L., with 5 and 6 years of working experience, respectively), blinded to the reconstruction information, independently evaluated the image quality using a slightly modified version of a method described previously [16]. First, overall image quality was scored as follows: 0, non-diagnostic; 1, numerous significant heterogeneities; 2, satisfactory, some significant heterogeneities of varying size and magnitude; 3, good, small heterogeneities visible throughout; 4, very good, subtle, tiny heterogeneities; or 5, excellent, no/minimal heterogeneities. Figure 2 shows typical images of scores 1–5. Second, the noise in the liver and the bone marrow was also scored visually using the same criteria.

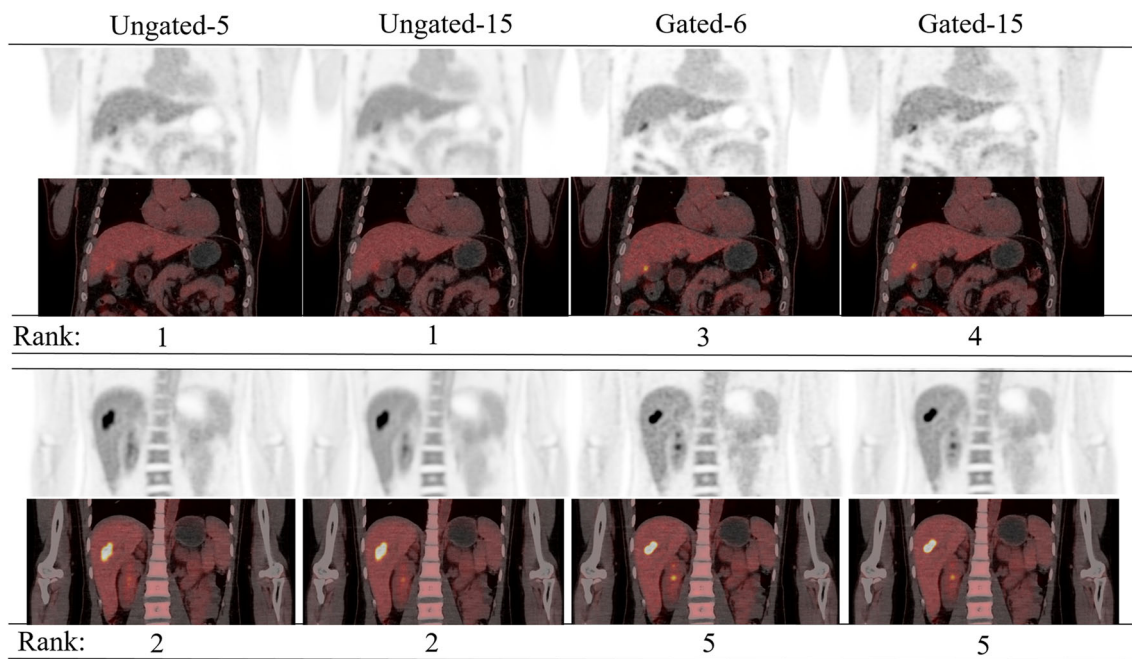


**Fig. 2** Coronal PET and fused PET/CT slices on an SUV grayscale of 0–6 from two representative cases illustrating subjective assessment of image qualities. The overall score is shown below each image

**Statistical analysis**

Statistical analysis was performed using the SPSS 20 (IBM Corp.). The weighted kappa was calculated to evaluate inter-rater agreement in subjective image analysis, while intra-class coefficients (ICC) were calculated to assess inter- and intra-operator agreements regarding quantitative measurements. Comparisons of quantitative indices among the four PET sets were performed using one-way ANOVA with repeated measures if the Kolmogorov–Smirnov test confirmed normality; otherwise, the Friedman test was used. The Cochran Q test was performed to compare lesion detectability among the four PET sets. For pairwise post hoc comparisons, the Bonferroni corrections were applied. Lesions were divided into two size groups (by median MTV), and two location groups (esophageal/pancreatic and others). Relative differences of lesions’ quantitative indices between Gated-15 and Ungated-15/5 were calculated as  $\frac{|Gated_{15}-Ungated_{15/5}|}{Gated_{15}} \times 100\%$ , and were compared between the two size and location groups, using the Mann–Whitney U test. All tests were two-sided, with  $p < 0.05$  indicating statistical significance.

**Results**

**Patient characteristics**

Table 1 summarizes the characteristics of the patients. All patients had confirmed the pathological diagnosis: 41

**Table 1** Basic and clinical information of the 71 patients included in this study

Characteristics	N = 71
Gender	
Male, n (%)	49 (69.0%)
Female, n (%)	22 (31.0%)
Age, years (mean ± SD)	58.9 ± 14.1
Height, cm (mean ± SD)	166.0 ± 7.3
Weight, kg (mean ± SD)	63.8 ± 10.7
Injected dose, MBq (mean ± SD)	278.9 ± 48.9
Mean glycemia, mmol/L (range)	6.1 (3.9–10.7)
Resting time post injection, min (mean ± SD)	60.2 ± 16.3
Method of final diagnosis	
Biopsy, n (%)	41 (57.7%)
Surgery, n (%)	30 (42.3%)
Lesion location and pathology*	
Lung cancer and metastasis, n (%)	24 (33.8%)
Liver cancer and metastasis, n (%)	25 (35.2%)
Esophageal cancer, n (%)	7 (9.9%)
Gastric cancer, n (%)	7 (9.9%)
Pancreatic cancer, n (%)	4 (5.6%)
Gallbladder cancer, n (%)	4 (5.6%)
Liver benign lesion, n (%)	2 (2.8%)
Lung benign lesion, n (%)	1 (1.4%)

SD, standard deviation; \*, the summed percentages of all types exceeds 100% because some patients had primary cancer as well as liver/lung metastasis

(57.7%) from biopsy and 30 (42.3%) from surgery. While 68 patients had malignant lesions, 3 had benign lesions.

### Respiratory gating, image reconstruction, and prompt counts

An average of 223.8 respiratory cycles were recorded for the 15-min gated imaging;  $18.0 \pm 16.8$  cycles failed for image reconstruction, leaving  $223.8 \pm 57.6$  (about 92.4%) cycles effective for respiratory-gating reconstruction (Table 2). The prompt counts of each image set were estimated as follows: count rates  $\times$  imaging time  $\times$  percentage of bins (1/3)  $\times$  percentage of effective respiratory cycles. Counts (including true, random, and scatter) were significantly lower in Gated-15 than in Ungated-15 and Ungated-5 (Table 2). However, the differences were not significant between Gated-15 and Gated-6. Interestingly, the proportion of effective counts was significantly higher in Gated-15 than in Ungated-15 (41.55% vs. 39.87%,  $p < 0.001$ ) and in Ungated-5 (41.55% vs. 41.08%,  $p < 0.001$ ). The proportion of effective counts was even higher in Gated-6 than in Gated-15 (41.95% vs. 41.55%,  $p < 0.001$ ).

### Objective assessments of background [ $^{18}\text{F}$ ]FDG uptake

Both the inter- and intra-operator agreements regarding SUV measurements of background [ $^{18}\text{F}$ ]FDG uptake were excellent ( $\text{ICC} > 0.85$ , Table S1). The mean SUVs in the background liver and blood pool were close among the four image sets, although most of the intergroup differences were statistically significant (Table 3). Liver  $\text{SUV}_{\text{SD}}$  and blood-pool  $\text{SUV}_{\text{SD}}$  were significantly higher in Gated-15 than in Ungated-15. This resulted in significantly lower SNR in the liver and blood pool in Gated-15 than in Ungated-15

and Ungated-5. Even worse results were seen in Gated-6 which, compared to Gated-15, had significantly higher liver  $\text{SUV}_{\text{SD}}$  (0.24 vs. 0.17,  $p < 0.001$ ) and blood-pool  $\text{SUV}_{\text{SD}}$  (0.16 vs. 0.10,  $p < 0.001$ ), and significantly lower liver SNR (9.79 vs. 14.20,  $p < 0.001$ ) and blood-pool SNR (10.80 vs. 15.87,  $p < 0.001$ ).

### Lesion detectability and [ $^{18}\text{F}$ ]FDG uptake

A total of 390 lesions were found in the thorax and upper abdomen (Table 4). Lesion detectability in gated-15 was significantly higher than in ungated-15 (97.2% vs. 93.6%,  $p = 0.001$ ) and Ungated-5 (97.2% vs. 92.3%,  $p = 0.001$ ), but comparable to that in Gated-6 (97.2% vs. 95.9%,  $p = 0.993$ ).

A total of 131 lesions were measured for quantitative analysis, with excellent inter- and intra-operator agreements ( $\text{ICC} > 0.90$ , Table S1). Lesions in Gated-15 presented significantly higher  $\text{SUV}_{\text{max}}$ ,  $\text{SUV}_{90\%}$ ,  $\text{SUV}_{\text{mean}}$ ,  $\text{SUV}_{\text{peak}}$ , TLR, and TBR, and significantly smaller MTV compared to Ungated-15 and Ungated-5 (Table 4). These differences remained even when only lung or liver lesions were considered (Table S2). In the subgroup analysis by lesion size (Fig. 3), the differences in the various quantifications between Gated-15 and Ungated-15 or Ungated-5 were more obvious among relatively smaller lesions ( $\text{MTV} \leq 4326.2$  mL) than among relatively larger lesions ( $\text{MTV} > 4326.2$  mL) of this study. Negative correlations had been found between the relative differences of the various quantifications with lesion volumes (Table S3). In the subgroup analysis by lesion location, lesions in the esophagus and pancreas presented relatively smaller differences in the quantifications between Gated-15 and Ungated-15 or Ungated-5, although none of the differences had reached statistically significant (Fig. 3). However, none of these indices

**Table 2** Summary statistics of the estimated counts and respiratory cycles among the four image sets

Variables	Gated-15	Ungated-15	Ungated-5	Gated-6	$p_0$	$p_1$	$p_2$	$p_3$
Respiratory cycles								
Total	$238.6 \pm 63.1$	-	-	$95.2 \pm 26.1$	-	-	-	-
Effective	$223.8 \pm 57.4$	-	-	$89.8 \pm 24.2$	-	-	-	-
Failed	$18.0 \pm 16.8$	-	-	$6.7 \pm 7.0$	-	-	-	-
Percent of effective	$92.4 \pm 6.9$			$92.7 \pm 7.6$				
Estimated counts (billion)								
True	$0.41 \pm 0.09$	$1.15 \pm 0.22$	$0.45 \pm 0.07$	$0.29 \pm 0.17$	$< 0.001^\dagger$	$< 0.001^\dagger$	$< 0.001^\dagger$	$> 0.999^\dagger$
Random	$0.96 \pm 0.36$	$2.40 \pm 0.83$	$1.09 \pm 0.37$	$0.73 \pm 0.53$	$< 0.001^\dagger$	$< 0.001^\dagger$	$< 0.001^\dagger$	$> 0.999^\dagger$
Scatter	$0.24 \pm 0.06$	$0.72 \pm 0.15$	$0.28 \pm 0.05$	$0.18 \pm 0.11$	$< 0.001^\dagger$	$< 0.001^\dagger$	$< 0.001^\dagger$	$> 0.999^\dagger$
Effective (true + scatter)	$0.65 \pm 0.13$	$1.87 \pm 0.36$	$0.73 \pm 0.11$	$0.48 \pm 0.29$	$< 0.001^\dagger$	$< 0.001^\dagger$	$< 0.001^\dagger$	$> 0.999^\dagger$
Percent of effective (%)	$41.55 \pm 4.88$	$39.87 \pm 4.60$	$41.08 \pm 4.90$	$41.95 \pm 4.95$	$< 0.001^\ddagger$	$< 0.001^\ddagger$	$< 0.001^\ddagger$	$< 0.001^\ddagger$

Data presented are mean  $\pm$  standard deviation.  $^\dagger$ , Freidman test;  $^\ddagger$ , One-way ANOVA with repeated measures.  $p_0$  indicates  $p$  values of one-way ANOVA with repeated measures or Freidman test among four groups;  $p_1$  to  $p_3$  indicates adjusted  $p$  values after Bonferroni corrections from comparisons between Gated-15 and Ungated-15, between Gated-15 and Ungated-5, and between Gated-15 and Gated-6, respectively

**Table 3** Comparisons of objective measurements of background uptake among the four PET image sets

Index	Total number	Gated-15	Ungated-15	Ungated-5	Gated-6	$p_0$	$p_1$	$p_2$	$p_3$
Liver SUV <sub>mean</sub>	71	2.30 ± 0.32	2.29 ± 0.33	2.36 ± 0.35	2.34 ± 0.32	< 0.001 <sup>†</sup>	0.099 <sup>†</sup>	< 0.001 <sup>†</sup>	< 0.001 <sup>†</sup>
Liver SUV <sub>SD</sub>	71	0.17 ± 0.03	0.10 ± 0.02	0.16 ± 0.03	0.24 ± 0.04	< 0.001 <sup>‡</sup>	< 0.001 <sup>‡</sup>	0.916 <sup>‡</sup>	< 0.001 <sup>‡</sup>
Liver SNR	71	14.20 ± 1.98	23.54 ± 3.94	15.04 ± 1.85	9.79 ± 1.37	< 0.001 <sup>†</sup>	< 0.001 <sup>†</sup>	< 0.001 <sup>†</sup>	< 0.001 <sup>†</sup>
Blood pool SUV <sub>mean</sub>	71	1.60 ± 0.32	1.61 ± 0.33	1.71 ± 0.36	1.66 ± 0.35	< 0.001 <sup>†</sup>	0.597 <sup>†</sup>	< 0.001 <sup>†</sup>	< 0.001 <sup>†</sup>
Blood pool SUV <sub>SD</sub>	71	0.10 ± 0.02	0.06 ± 0.02	0.10 ± 0.02	0.16 ± 0.03	< 0.001 <sup>‡</sup>	< 0.001 <sup>‡</sup>	< 0.999 <sup>‡</sup>	< 0.001 <sup>‡</sup>
Blood pool SNR	71	15.87 ± 3.46	26.6 ± 6.24	16.77 ± 3.06	10.80 ± 2.02	< 0.001 <sup>†</sup>	< 0.001 <sup>†</sup>	0.032 <sup>†</sup>	< 0.001 <sup>†</sup>

Data are presented as mean ± standard deviation for continuous variables. †, One-way ANOVA with repeated measures. ‡, Freidman test.  $p_0$  indicates  $p$  values of one-way ANOVA with repeated measures or Freidman test among four groups;  $p_1$  to  $p_3$  indicates adjusted  $p$  values after Bonferroni corrections from comparisons between Gated-15 and Ungated-15, between Gated-15 and Ungated-5, and between Gated-15 and Gated-6, respectively

was statistically different between Gated-15 and Gated-6 ( $p_3$  in Table 4).

Figure 6 shows a typical case of the bone-marrow noise and liver noise in the four reconstructed PET images.

**Subjective assessments of image quality**

Inter-rater consistency in assessing the image quality was good (weighted kappa > 0.75; Table 5). Obviously, higher overall scores were identified in gated images than in ungated images, but no significant difference was found between Gated-15 and Gated-6 (4.77 vs. 4.62,  $p > 0.999$ ). Figure 4 and Figure 5 show typical cases of better presentation in gated images than in ungated images of lung and liver lesions. Although the scores for liver noise and bone-marrow noise were significantly lower in Gated-15 (4.15 and 4.38, respectively) than in Ungated-15 (4.93 and 4.92, respectively), they were comparable to the scores in Ungated-5 (4.30 and 4.43, respectively) (Table 5). However, liver noise (3.16 vs. 4.15,  $p < 0.001$ ) and bone-marrow noise (3.57 vs. 4.38,  $p < 0.001$ ) were significantly higher in Gated-6 than in Gated-15.

**Discussion**

In this study, we investigated the performance of respiratory-gated total-body PET/CT in a patient cohort with miscellaneous suspect malignancies. The 15-min gated PET imaging outperformed the 15-min ungated and the 5-min “count-matched” ungated PET imaging, in lesion detectability, presentation, and quantification, with comparable overall image quality. Despite the reduced acquisition time of 6 min, respiratory-gated imaging performed as well as 15-min gated imaging.

The results of this study show significance to the clinic. According to the European guideline, for traditional full-activity imaging (~3.7 MBq/kg), a PET system with short AFOV of 15–25 cm and an imaging protocol with a bed overlap of > 30% and an acquisition time of 2 min/bed for the body

**Table 4** Comparisons of objective measurements of lesions among the four PET image sets

Index	Total number	Gated-15	Ungated-15	Ungated-5	Gated-6	$p_0$	$p_1$	$p_2$	$p_3$
Lesion detected (%)	390	379 (97.2%)	365 (93.6%)	360 (92.3%)	374 (95.9%)	< 0.001*	0.001*	0.001*	0.993*
Lesion uptake									
SUV <sub>max</sub>	131	11.41 ± 5.49	10.17 ± 5.00	10.24 ± 5.05	11.59 ± 5.67	< 0.001 <sup>†</sup>	< 0.001 <sup>†</sup>	< 0.001 <sup>†</sup>	> 0.999 <sup>†</sup>
SUV <sub>mean</sub>	131	6.23 ± 2.78	5.67 ± 2.53	5.66 ± 2.46	6.23 ± 2.78	< 0.001 <sup>†</sup>	< 0.001 <sup>†</sup>	< 0.001 <sup>†</sup>	> 0.999 <sup>†</sup>
SUV <sub>90%</sub>	107 <sup>a</sup>	11.06 ± 5.45	9.67 ± 5.06	9.82 ± 4.97	11.70 ± 5.69	< 0.001 <sup>†</sup>	< 0.001 <sup>†</sup>	< 0.001 <sup>†</sup>	> 0.999 <sup>†</sup>
SUV <sub>peak</sub>	114 <sup>b</sup>	9.25 ± 4.59	8.59 ± 4.32	8.45 ± 4.42	9.20 ± 4.72	< 0.001 <sup>†</sup>	< 0.001 <sup>†</sup>	< 0.001 <sup>†</sup>	0.412 <sup>†</sup>
MTV, ×1000 mL	131	24.48 ± 60.78	26.26 ± 62.61	26.05 ± 63.60	23.91 ± 58.50	< 0.001 <sup>†</sup>	< 0.001 <sup>†</sup>	< 0.001 <sup>†</sup>	> 0.999 <sup>†</sup>
TLR	131	5.04 ± 2.54	4.57 ± 2.44	4.46 ± 2.37	5.06 ± 2.62	< 0.001 <sup>†</sup>	< 0.001 <sup>†</sup>	< 0.001 <sup>†</sup>	> 0.999 <sup>†</sup>
TBR	131	7.41 ± 4.13	6.61 ± 3.80	6.28 ± 3.67	7.30 ± 4.22	< 0.001 <sup>†</sup>	< 0.001 <sup>†</sup>	< 0.001 <sup>†</sup>	0.231 <sup>†</sup>

Data are presented as mean ± standard deviation for continuous variables. †, Freidman test; \*, Cochran Q test.  $p_0$  indicates  $p$  values of Freidman test or Cochran Q test among four groups;  $p_1$  to  $p_3$  indicates adjusted  $p$  values after Bonferroni corrections from comparisons between Gated-15 and Ungated-15, between Gated-15 and Ungated-5, and between Gated-15 and Gated-6, respectively; a, 24 lesions failed to obtain SUV<sub>90%</sub> because of small size and narrow distribution of voxel uptake; b, 17 lesions failed to obtain SUV<sub>peak</sub> because of small size

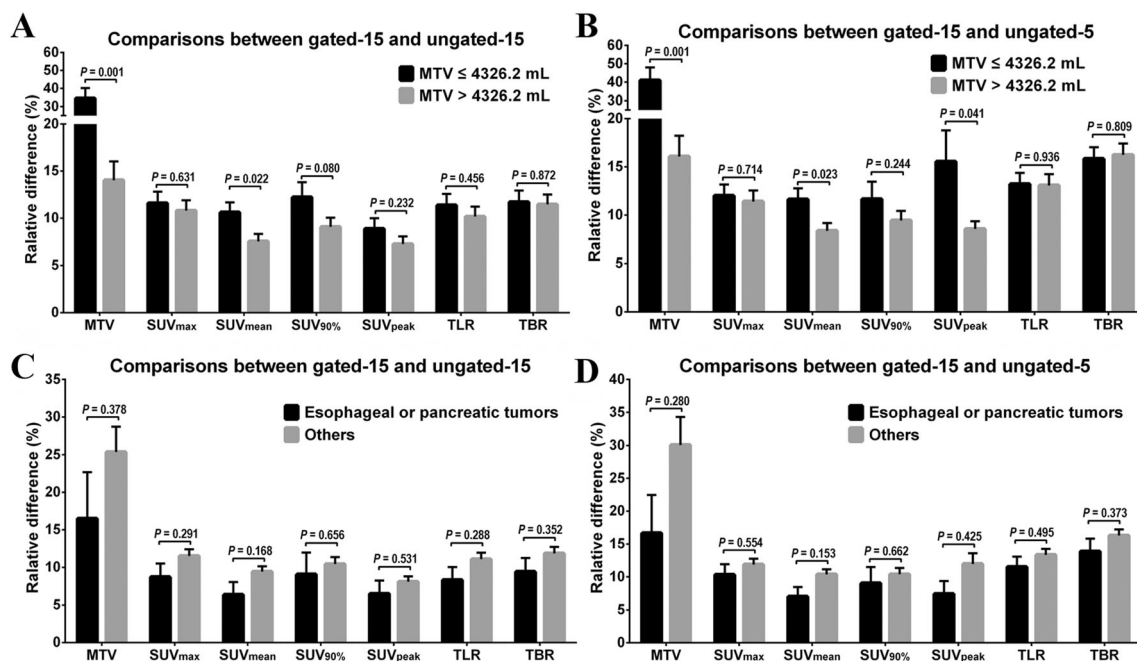


**Fig. 3** Comparisons of the gated-to-ungated differences of lesion quantifications between lesions of MTV > 4326.2 mL and ≤ 4326.2 mL (A and B), and between lesions from the esophagus/pancreas and those from

other places (C and D). A and C, Differences between Gated-15 and Ungated-15. C and D, Differences between Gated-15 and Ungated-5

and 5 min/bed for the brain, would require an acquisition time over 15 min for a whole-body PET imaging [13]. If respiratory gating were to be applied for the two bed positions in the upper abdomen and lower thorax, the acquisition time would be tripled with the use of hardware-based gating [17] or doubled with the use of data-driven gating [7]; a total time of 19–23 min would be required. This is not a suitable protocol for oncological imaging, especially in seriously ill patients who cannot tolerate prolonged immobilization. The reduced time of 6 min for respiratory-gated total-body PET imaging, as identified in our study, would be more practical in the clinic. This result is consistent with our previous experience in

ungated total-body PET imaging as the Gated-6 just matched the count of the 2-min protocol recommended for a full-activity ungated imaging [12].

A cost of respiratory gating is the reduced counts for image reconstruction with increased image noise. In our study, increased noise in the liver and blood pool leading to reduced SNR of image were identified in gated images compared to ungated images. In addition, the subjective scores of liver and bone marrow noise were lower in Gated-15 than in Ungated-15. The image SNR and subjective scores of noise were even lower in Gated-6. However, SNR of background liver in both Gated-15 ( $14.20 \pm 1.98$ ) and Gated-6 ( $9.79 \pm 1.37$ ) were

**Table 5** Subjective assessment of the image qualities and the inter-rater consistency among the four PET image sets

Subjective scores	Gated-15	Ungated-15	Ungated-5	Gated-6	$p_0$	$p_1$	$p_2$	$p_3$
Overall	$4.77 \pm 0.48$	$3.55 \pm 1.28$	$3.57 \pm 1.26$	$4.62 \pm 0.64$	$< 0.001^\ddagger$	$< 0.001^\ddagger$	$< 0.001^\ddagger$	$> 0.999^\ddagger$
Liver noise	$4.15 \pm 0.57$	$4.93 \pm 0.34$	$4.30 \pm 0.57$	$3.16 \pm 0.57$	$< 0.001^\ddagger$	$< 0.001^\ddagger$	$> 0.999^\ddagger$	$< 0.001^\ddagger$
Bone marrow noise	$4.38 \pm 0.59$	$4.92 \pm 0.36$	$4.43 \pm 0.70$	$3.57 \pm 0.66$	$< 0.001^\ddagger$	$0.001^\ddagger$	$> 0.999^\ddagger$	$< 0.001^\ddagger$
Weighted kappa (95% CI)								
Overall	0.789 (0.640–0.939)	0.785 (0.699–0.870)	0.767 (0.674–0.860)	0.819 (0.694–0.943)				
Liver noise	0.906 (0.710–1.000)	0.838 (0.711–0.964)	0.770 (0.619–0.921)	0.782 (0.638–0.926)				
Bone marrow noise	0.751 (0.593–0.898)	0.825 (0.562–1.000)	0.817 (0.699–0.936)	0.794 (0.670–0.917)				

Note: Data are presented as mean  $\pm$  standard deviation for subjective scores. CI, confidence interval.  $^\ddagger$ , Freidman test.  $p_0$  indicates  $p$  values of the Freidman test among four groups;  $p_1$  to  $p_3$  indicates adjusted  $P$  values after Bonferroni corrections from comparisons between Gated-15 and Ungated-15, between Gated-15 and Ungated-5, and between Gated-15 and Gated-6, respectively

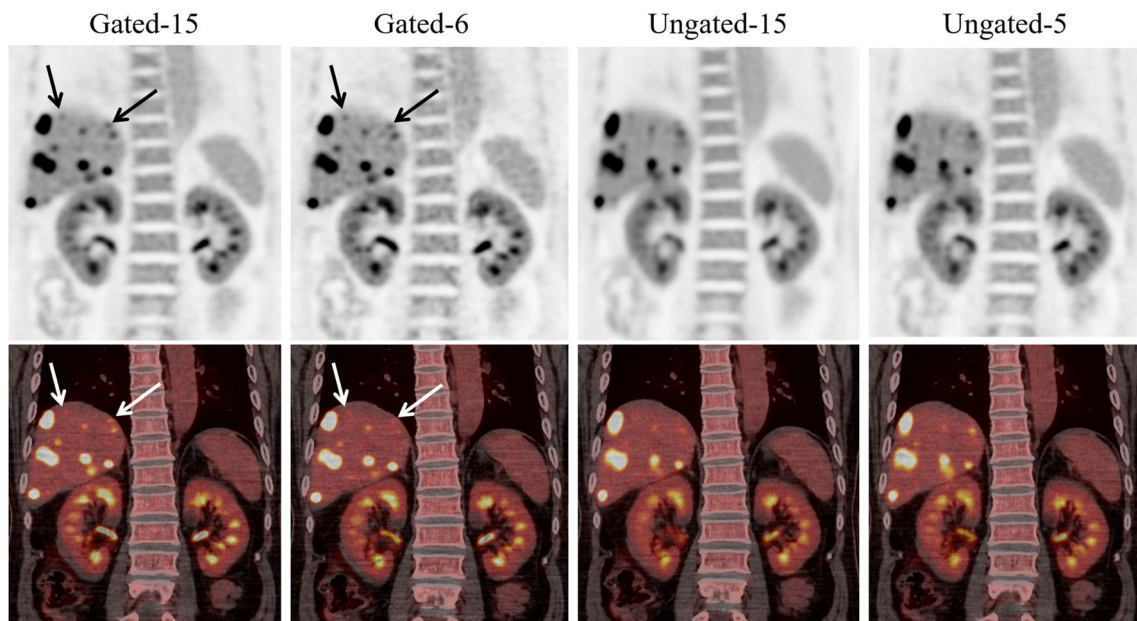


**Fig. 4** Coronal slices of PET and fused PET/CT (SUV grayscale, 0–6) showing [<sup>18</sup>F]FDG-avid liver metastasis (arrows), which are easier to visualize on gated reconstructions but not definitely visible on Ungated-15

and Ungated-5 images. The Gated-15 and Gated-6 images received a score of 5 and 4, respectively, while Ungated-15 and Ungated-5 both received an overall score of 1

relative high when compared to the SNR in PET images (full-activity, 2 min/bed) with clinically acceptable qualities (liver SNR:  $8.3 \pm 1.2$ ) obtained using conventional PET scanner with the state-of-art configurations [18]. Furthermore, when compared with total-body PET images in our previous studies, the SNR of background liver and blood pool, and the subjective scores of liver noise in both Gated-15 and Gated-6, exceeded the corresponding results of 2-min full-activity

images and fulfilled the requirement for clinical diagnosis [19, 20]. One method to reduce noise is to increase the injected activity to gain better counting statistics for compensating the count loss caused by failure of respiration capture. This is why we used a relatively higher dose of [<sup>18</sup>F]FDG (4.4 MBq/kg instead of 3.7 MBq/kg) [13]. Another method to reduce image noise is to reduce the number of iterations to two; we are exploring this possibility also.

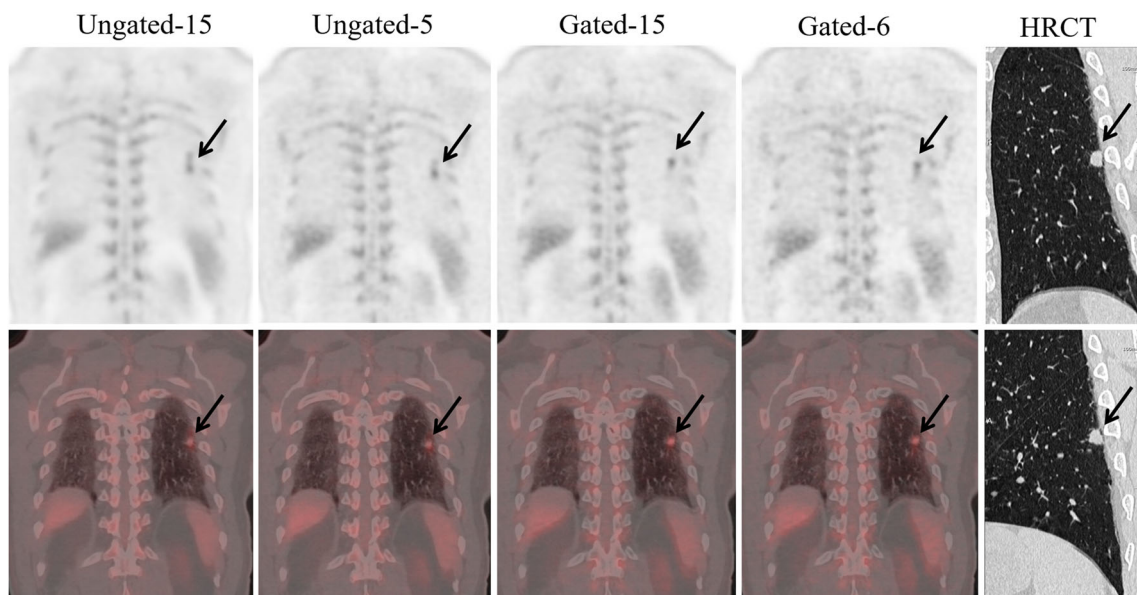
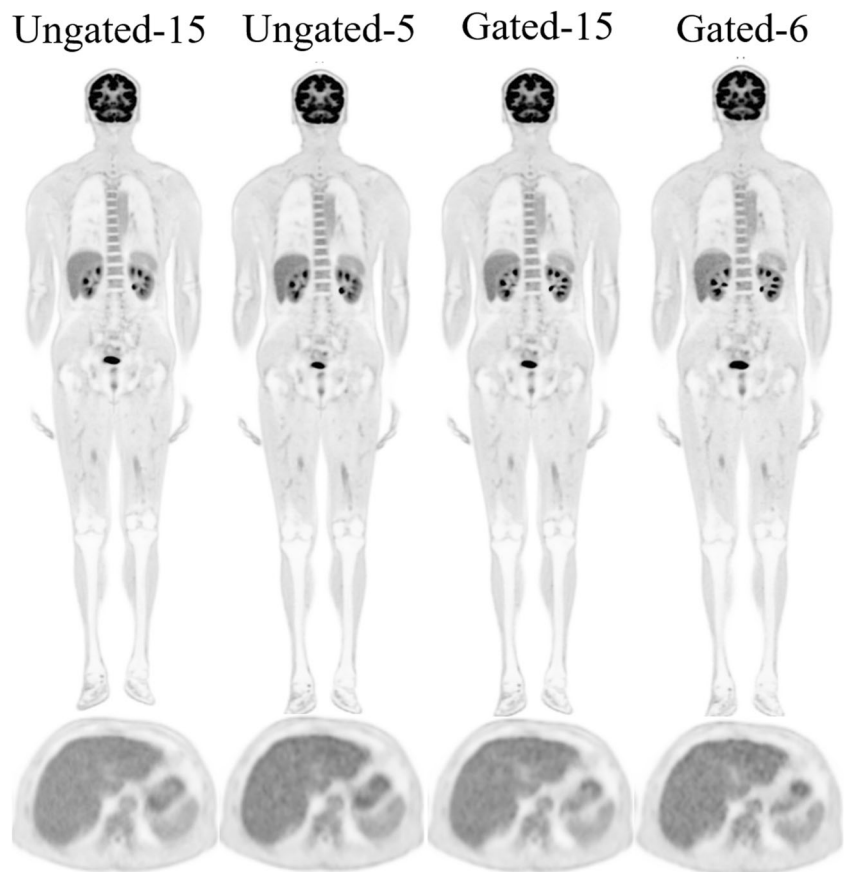


**Fig. 5** Coronal slices of PET, fused PET/CT and breath-hold high-resolution CT (HRCT: upper coronal; lower, sagittal) showing an [<sup>18</sup>F]FDG-avid lung cancer with obvious deformation on ungated images. This lesion can be easily misdiagnosed as two lesions on Ungated-15 and

Ungated-5, which received an overall score of 2 and 1, respectively. The deformation is markedly less on Gated-15 and Gated-6 images, which received overall scores of 5 and 4, respectively. The PET images are on an SUV grayscale of 0–6



**Fig. 6** Coronal (upper row) and axial (lower row) slices of PET showing bone-marrow noise and liver noise, respectively. The bone-marrow noise is comparable among the four image sets, and thus all received a subjective score of 5. The liver noise is close among Ungated-5, Gated-15, and Gated-6, which is slightly inferior to Ungated-15; thus, subjective scores of 5, 4, 4, and 4 were given to these four image sets, respectively. The images are on an SUV grayscale of 0–6



Another important factor that hinders the clinical application of respiratory gating is the strict requirement for regular respiration. In our study cohort, approximately 7.6% of respiratory cycles were unavailable for use in image reconstruction. The proportion would be much higher for seriously ill oncology patients whose respiration can be very disordered.

As for image counts, it is reported that at least 10 million true counts are required for the accurate quantification of lung lesions on PET images [21]. Schaefferkoetter et al found that for obtaining image quality and lesion detection equal to that with full-count imaging, the minimum requirement was 5 million effective counts [22]. In our study, the mean true counts of Gated-15 and Gated-6 were 410 and 290 million, respectively, and the mean effective counts were 650 and 480 million, respectively, which were both significantly higher than these requirements. Interestingly, the gated images presented significantly higher percentages of effective counts than in ungated images in our study (Table 2). This might have compensated for the reduced total counts and led to the comparable subjective liver- and bone-marrow-noise scores in Gated-15 and Ungated-5. Given the dramatically high amount of counts detected, it is likely that the acquisition time can be reduced further if the data-driven-gating technique is used [16].

In PET/CT imaging, malignant lesions commonly show higher tracer uptake than adjacent areas. Therefore, for small lesions, the respiratory motion would cause the measured prompts to be lower as a larger amount of adjacent normal areas would be included than would be the case with large lesions. In our study, more obvious underestimations of quantification in ungated imaging were found in relatively small lesions; this is consistent with previous studies [23, 24]. Another factor affecting the efficiency of respiratory gating is the lesion location. For example, lesions in the mediastinum or retroperitoneum are relatively invulnerable to respiration motion compared to lesions in other areas; this was confirmed in our study.

Several limitations of this study should be mentioned. First, we did not investigate how much further the acquisition time of respiratory-gated imaging could be reduced without compromising image quality. Nevertheless, a total time of 6 min for a total-body respiratory-gating PET imaging is dramatic. Second, the slightly higher dose of tracer used in this study increases radiation to the patient. However, the increase of tracer activity from 3.7 to 4.4 MBq/kg would only bring about an increase of 0.0133 mSv/kg of radiation, i.e., accounting for about 0.8 mSv for a 60-kg patient as calculated by the method suggested in the ICRP Publication 106 [25]; this slight

increase of radiation may not be a major concern for patients with malignancies. Third, we did not include patients without pathologically confirmed diagnosis aiming to confine the study subjects to be a patient set with definitive diagnosis in order to guarantee a robust result that could be likely extrapolated to similar patients from other institutions using similar PET/CT scanner. Finally, we did not apply the data-driven-gating technique, although its great potential in total-body PET imaging has been indicated in recent studies [16, 26].

To conclude, [ $^{18}\text{F}$ ]FDG PET/CT imaging using the total-body PET scanner allows for respiratory-gated imaging with dramatically reduced scanning time while providing image quality superior to that obtained with ungated time- or count-matched imaging. Therefore, there should be increased use of respiratory gating in clinical PET imaging.

**Supplementary Information** The online version contains supplementary material available at <https://doi.org/10.1007/s00330-022-09369-z>.

**Funding** This study was funded by the Shanghai “Rising Stars of Medical Talent”–Youth Development Program (grant number: HWJRS2019-72 to G.L.), the Shanghai Municipal Key Clinical Specialty Project (grant number: SHSLCZDZK03401 to H.S.), the Major Science and Technology Projects for Major New Drug Creation (grant number: 2019ZX09302001 to H.S.), the Shanghai Science and Technology Committee Program (grant number: 20DZ2201800 to H.S.), the Three-year Action Plan of Clinical Skills and Innovation of Shanghai Hospital Development Center (grant number: SHDC2020CR3079B to H.S.), and the Next Generation Information Infrastructure Construction Project founded by Shanghai Municipal Commission of Economy and Informatization (grant number: 201901014 to H.S.).

## Declarations

**Guarantor** The scientific guarantor of this publication is Hongcheng Shi.

**Conflict of interest** The authors of this manuscript declare no relationships with any companies whose products or services may be related to the subject matter of the article.

**Statistics and biometry** One of the authors has significant statistical expertise.

**Informed consent** Written informed consent was obtained from all patients in this study.

**Ethical approval** Institutional Review Board approval was obtained.

## Methodology

- prospective
- diagnostic
- performed at one institution

## References

1. Keall PJ, Mageras GS, Balter JM et al (2006) The management of respiratory motion in radiation oncology report of AAPM Task Group 76. *Med Phys* 33:3874–3900
2. Nehmeh SA, Erdi YE, Ling CC et al (2002) Effect of respiratory gating on quantifying PET images of lung cancer. *J Nucl Med* 43: 876–881
3. Büther F, Vehren T, Schäfers KP, Schäfers M (2016) Impact of data-driven respiratory gating in clinical PET. *Radiology* 281: 229–238
4. Suzawa N, Ichikawa Y, Ishida M, Tomita Y, Nakayama R, Sakuma H (2016) Respiratory-gated time-of-flight PET/CT during whole-body scan for lung lesions: feasibility in a routine clinical setting and quantitative analysis. *Ann Nucl Med* 30:722–730
5. Guerra L, De Ponti E, Elisei F et al (2012) Respiratory gated PET/CT in a European multicentre retrospective study: added diagnostic value in detection and characterization of lung lesions. *Eur J Nucl Med Mol Imaging* 39:1381–1390
6. Dawood M, Buther F, Lang N, Schober O, Schafers KP (2007) Respiratory gating in positron emission tomography: a quantitative comparison of different gating schemes. *Med Phys* 34:3067–3076
7. Liu C, Alessio A, Pierce L et al (2010) Quiescent period respiratory gating for PET/CT. *Med Phys* 37:5037–5043
8. Badawi RD, Shi H, Hu P et al (2019) First Human Imaging Studies with the EXPLORER Total-Body PET Scanner. *J Nucl Med* 60: 299–303
9. Alberts I, Hunermund JN, Prenosil G et al (2021) Clinical performance of long axial field of view PET/CT: a head-to-head intra-individual comparison of the Biograph Vision Quadra with the Biograph Vision PET/CT. *Eur J Nucl Med Mol Imaging* 48: 2395–2404
10. Hu P, Zhang Y, Yu H et al (2021) Total-body  $^{18}\text{F}$ -FDG PET/CT scan in oncology patients: how fast could it be? *Eur J Nucl Med Mol Imaging* 48:2384–2394
11. Liu G, Hu P, Yu H et al (2021) Ultra-low-activity total-body dynamic PET imaging allows equal performance to full-activity PET imaging for investigating kinetic metrics of  $^{18}\text{F}$ -FDG in healthy volunteers. *Eur J Nucl Med Mol Imaging* 48:2373–2383
12. Sui X, Liu G, Hu P et al (2021) Total-body PET/computed tomography highlights in clinical practice: experiences from Zhongshan Hospital, Fudan University. *PET Clin* 16:9–14
13. Boellaard R, Delgado-Bolton R, Oyen WJ et al (2015) FDG PET/CT: EANM procedure guidelines for tumour imaging: version 2.0. *Eur J Nucl Med Mol Imaging* 42:328–354
14. Boudraa A, Zaidi H (2006) Image segmentation techniques in nuclear medicine imaging. In: Zaidi H (ed) *Quantitative analysis in nuclear medicine imaging*. Springer, New York, pp 308–357
15. Foster B, Bagci U, Mansoor A, Xu Z, Mollura DJ (2014) A review on segmentation of positron emission tomography images. *Comput Biol Med* 50:76–96
16. Walker MD, Morgan AJ, Bradley KM, McGowan DR (2020) Data-driven respiratory gating outperforms device-based gating for clinical  $^{18}\text{F}$ -FDG PET/CT. *J Nucl Med* 61:1678–1683
17. van Elmpt W, Hamill J, Jones J, De Ruyscher D, Lambin P, Ollers M (2011) Optimal gating compared to 3D and 4D PET reconstruction for characterization of lung tumours. *Eur J Nucl Med Mol Imaging* 38:843–855
18. Tan H, Sui X, Yin H et al (2021) Total-body PET/CT using half-dose FDG and compared with conventional PET/CT using full-dose FDG in lung cancer. *Eur J Nucl Med Mol Imaging* 48: 1966–1975
19. Zhang Y, Hu P, Wu R et al (2020) The image quality, lesion detectability, and acquisition time of  $^{18}\text{F}$ -FDG total-body PET/CT in oncological patients. *Eur J Nucl Med Mol Imaging* 47:2507–2515

20. Hu P, Zhang Y, Yu H et al (2021) Total-body  $^{18}\text{F}$ -FDG PET/CT scan in oncology patients: how fast could it be? *Eur J Nucl Med Mol Imaging* 48:2384–2395
21. Schaefferkoetter JD, Yan J, Sjöholm T et al (2017) Quantitative accuracy and lesion detectability of low-dose  $^{18}\text{F}$ -FDG PET for lung cancer screening. *J Nucl Med* 58:399–405
22. Schaefferkoetter JD, Yan J, Townsend DW, Conti M (2015) Initial assessment of image quality for low-dose PET: evaluation of lesion detectability. *Phys Med Biol* 60:5543–5556
23. Werner MK, Parker JA, Kolodny GM, English JR, Palmer MR (2009) Respiratory gating enhances imaging of pulmonary nodules and measurement of tracer uptake in FDG PET/CT. *AJR Am J Roentgenol* 193:1640–1645
24. Farid K, Poullias X, Alifano M et al (2015) Respiratory-gated imaging in metabolic evaluation of small solitary pulmonary nodules:  $^{18}\text{F}$ -FDG PET/CT and correlation with histology. *Nucl Med Commun* 36:722–727
25. ICRP (2008) Radiation dose to patients from radiopharmaceuticals. Addendum 3 to ICRP Publication 53. ICRP Publication 106. Approved by the Commission in October 2007. *Ann ICRP* 38:1–197
26. Tumpa TR, Acuff SN, Gregor J, Lee S, Hu D, Osborne DR (2021) A data-driven respiratory motion estimation approach for PET based on time-of-flight weighted positron emission particle tracking. *Med Phys* 48:1131–1143

**Publisher's note** Springer Nature remains neutral with regard to jurisdictional claims in published maps and institutional affiliations.

Springer Nature or its licensor (e.g. a society or other partner) holds exclusive rights to this article under a publishing agreement with the author(s) or other rightsholder(s); author self-archiving of the accepted manuscript version of this article is solely governed by the terms of such publishing agreement and applicable law.